Atmospheric Environment 183 (2018) 165–174

Contents lists available at ScienceDirect

Atmospheric Environment

journal homepage: www.elsevier.com/locate/atmosenv

Long-term systematic profiling of dust aerosol optical properties using the EOLE NTUA lidar system over Athens, Greece (2000–2016)

O. Soupiona[a,*], A. Papayannis[a], P. Kokkalis[a,b], M. Mylonaki[a], G. Tsaknakis[a], A. Argyrouli[c,d], S. Vratolis[a,e]

[a] Laser Remote Sensing Unit, Physics Department, School of Applied Mathematics and Physical Sciences, National Technical University of Athens, 15780, Zografou, Greece
[b] Remote Sensing Group, Department of Physics, Kuwait University, P.O. Box 5969, Safat, 13060, Kuwait
[c] Technical University of Munich, Department of Civil, Geo and Environmental Engineering, Chair of Remote Sensing Technology, Munich, Germany
[d] German Aerospace Centre (DLR), Remote Sensing Technology Institute, Oberpfaffenhofen, 82234, Wessling, Germany
[e] ERL, Institute of Nuclear & Radiological Sciences & Technology, Energy & Safety, National Centre of Scientific Research Demokritos, 15310, Ag. Paraskevi, Attiki, Greece

GRAPHICAL ABSTRACT

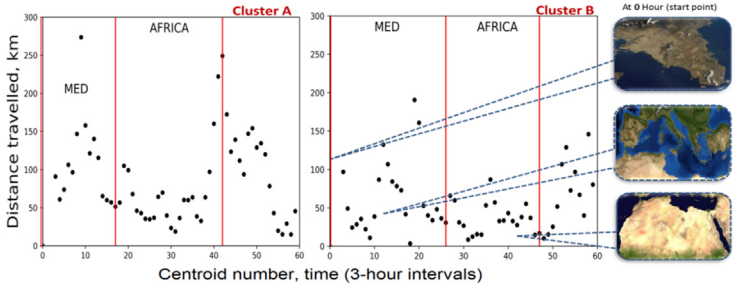

ARTICLE INFO

Keywords:
Aerosols
Dust
Lidar
Aging
Athens
Greece

ABSTRACT

We present a comprehensive analysis of the seasonal variability of the vertical profiles of the optical and geometrical properties of Saharan dust aerosols, observed in the height region between 1000 and 6000 m, over the city of Athens, Greece, from February 2000 to December 2016. These observations were performed by a multi-wavelength (355-387-532-1064 nm) Raman lidar system under cloud-free conditions. The statistical analysis (using aerosol monthly mean values) is based on nighttime vertical Raman measurements of range-resolved aerosol optical properties (backscatter and extinction coefficients, lidar ratio, Ångström exponent) at 355 nm (57 dust events during more than 80 measurement hours). We found that the number of dust events was highest in spring, summer, and early autumn periods and that during spring the dust layers were moved at higher altitudes (~4500 m) than in other seasons. The number of the forecasted dusty days (on monthly basis) by the BSC-DREAM8b model compared to those of the performed lidar measurements were found to have a quite strong correlation (R^2 = 0.81), with a maximum occurrence predicted for the spring season. In the worst case scenario, at least 50% of the model-forecasted dust events can be observed by lidar under cloudless skies over Athens. For the sampled dust plumes we found mean lidar ratios of 52 ± 13 sr at 355 nm in the height range 2000–4000 m a.s.l. Moreover, the dust layers had a mean thickness of 2497 ± 1026 m and a center of mass of 2699 ± 1017 m.

An analysis performed regarding the air mass back-trajectories arriving over Athens revealed two main clusters: one pathway from south-west to north-east, with dust emission areas in Tunisia, Algeria and Libya and a second one from south, across the Mediterranean Sea with emission areas over Libya and the remaining part of Algeria and Tunisia. This clustering enabled us to differentiate between the aerosol optical properties between

* Corresponding author.
E-mail address: soupiona.rania@gmail.com (O. Soupiona).

https://doi.org/10.1016/j.atmosenv.2018.04.011
Received 9 October 2017; Received in revised form 5 April 2018; Accepted 8 April 2018
Available online 14 April 2018

the two clusters, based on their residence time over the Saharan region, the European continent and the Mediterranean Sea. We finally concluded that even if the dust source regions are about the same, the aging and mixing processes of these air masses, passing over different areas, might have an impact on the aerosol optical properties.

1. Introduction

Dust aerosols have a great impact on the Earth's radiation budget, both directly and indirectly: directly by scattering and absorbing solar and terrestrial thermal radiation, indirectly by acting as cloud condensation nuclei (CCN) influencing clouds' microphysical and optical properties and lifetimes (Forster et al., 2007; Atkinson et al., 2013; IPCC, 2014; Seinfeld et al., 2016; Karydis et al., 2017). The African continent, especially its northern part (Sahara desert), is considered as the largest dust-producing region in the world (Prospero et al., 2002; Evan et al., 2016). Desert dust originated from Sahara is frequently lifted in the atmosphere and can be transported over long distances under specific weather conditions (Murayama et al., 2001; Knippertz and Todd, 2012; Marinou et al., 2017). Specifically, it is well known that a large amount of Saharan dust is transported over this part of the Mediterranean Sea, mainly because of cyclone activity inside and around the area (Prospero, 1996; Dunion et al., 2004; Gkikas et al., 2015). Athens is located in the north eastern Mediterranean, an area frequently exposed to transported Saharan dust (Papayannis et al., 2005, 2008, 2014; Tsekeri et al., 2013).

Before the establishment of the EARLINET (European Aerosol Research Lidar Network) (Pappalardo et al., 2014), the Saharan dust transportation over Europe through the Mediterranean region was systematically studied mainly by satellite observations (Dulac et al., 1992; Prospero, 1996; Moulin et al., 1997a,b) and ground-based sun photometers (Holben et al., 2001) and much less by lidar instruments employed during dedicated atmospheric field campaigns (e.g. Hamonou et al., 1999). Since the year 2000, when EARLINET was established, aerosol lidar measurements are carried out in Athens following the EARLINET measuring protocol (Bösenberg et al., 2003).

The laser remote sensing (lidar) technique is the most suitable tool for the retrieval of the vertical profiles of the aerosol optical properties, from the lower troposphere up to the stratosphere, with high temporal and spatial resolution (Amiridis et al., 2005; Balis et al., 2006; Papayannis et al., 2007; Mattis et al., 2008; Mona et al., 2006; Zuev et al., 2017). Moreover, using aerosol optical data, the retrieval of the corresponding aerosol microphysical properties is possible by using mathematical inversion codes (Samaras et al., 2015; Müller et al., 2016).

Lidar systems, operated in the Eastern Mediterranean, revealed that dust events over the region mostly occur from early spring to early autumn, while during winter months dust transport over the area remains quite low (Balis et al., 2004; Amiridis et al., 2005; Papayannis et al., 2005, 2008). Due to the proximity of Athens to the Saharan desert, the direct transport of dust is possible in some cases, only under specific meteorological conditions. Nevertheless, in most cases, the mineral dust is mixed with other components, like marine, continental, urban or biomass burning particles during the air masses overpass over the sea and continental regions (Papayannis et al., 2014).

The main aim of this work is to present a statistical analysis of aerosol optical and geometrical properties during Saharan dust events over Athens, Greece for the time-period 2000–2016. Since May 2000, our station has performed systematic lidar observations of the vertical profiles of dust aerosols over Athens on a coherent network basis within EARLINET. In Section 2, we briefly present the instrumentation and methodology used, while a brief description of the BSC Dust Regional Atmospheric Model (BSC/DREAM8b; cf. Basart et al., 2012) is also presented. Section 3 is devoted mainly to the statistical analysis of the dust events observed over Athens, Greece. Finally, our conclusions are given in Section 4.

2. Instrumentation and methodology

2.1. Raman lidar system (EOLE)

The (EOLE) (aErosol and Ozone Lidar systEm) Raman lidar system of the National Technical University of Athens (NTUA) operates since February 2000, as a member of the EARLINET, in compliance with the networks' quality assurance criterions and standards, both at hardware and software level (Böckmann et al., 2004; Matthais et al., 2004a,b; Freudenthaler, 2008; Pappalardo et al., 2014). EOLE is located at the Laser Remote Sensing Unit (LRSU) of NTUA (37.97° N, 23.79° E, elev. 212 m a.s.l.) and is an advanced 6-wavelength Raman lidar system capable of performing independent and simultaneous measurements of the vertical profiles of the aerosol backscatter (b_{aer} at 355, 532 and 1064 nm) and extinction (a_{aer} at 355 and 532 nm) coefficients. The emission unit of EOLE is based on a Nd:YAG laser, emitting high energy laser pulses at 355, 532 and 1064 nm with a repetition rate of 10 Hz. The receiving unit is able to detect the elastic backscatter lidar signals at 355-532-1064 nm and the Raman backscattered ones by the atmospheric N_2 at 387 nm (and 607 nm after the year 2010). The geometrical specification of EOLE makes feasible the full overlap of the laser beam with the receiver field of view to be reached at heights of the order of 800 m a.s.l. (Kokkalis et al., 2012; Kokkalis, 2017). Therefore, in this study the lidar data are presented for heights above 850 m a.s.l., where full overlap of the lidar system occurs.

During day-time measurements, only the b_{aer} (Klett, 1981, 1985) can be retrieved. The appropriate value of the constant lidar ratio (LR) (where $LR = a_{aer}/b_{aer}$) required as input, is constrained to the mean columnar aerosol optical depth (AOD) obtained from a nearby sunphotometer (e.g. Landulfo et al., 2007). Thus, the typical uncertainty of the retrieved b_{aer} vertical profile (including both statistical and systematic errors and corresponding to 30–60 min temporal resolution) is of the order of 20–30% (Bösenberg et al., 1997; Böckmann et al., 2004). The corresponding Ångström exponent (AE) related to b_{aer} values can be retrieved with a typical uncertainty of 25%. In case that nearby sunphotometric data are missing, we use lidar ratio values, related to the sampled air masses containing dust particles, provided by long-term Raman lidar measurements over Athens (Papayannis et al., 2008).

During nighttime measurements, the Raman technique is used as proposed by Ansmann et al. (1992) to retrieve the a_{aer} and b_{aer} aerosol vertical profiles, with systematic uncertainties of ~5–15% and ~10–25%, respectively (Ansmann et al., 1992; Mattis et al., 2002). Therefore, the corresponding systematic uncertainty of the retrieved lidar ratio values is of the order of 5–10%, while the mean uncertainty for AEs is of the order of ± 0.3.

2.2. Lidar data processing

The aerosol-related physical quantities used in this study, are the data products obtained from (a) manual and (b) automatic processing schemes; (a) The manual retrievals are based on the signal processing algorithms developed within EARLINET and tested during several intercomparisons (Böckmann et al., 2004; Matthais et al., 2004a; Pappalardo et al., 2014). This scheme has been applied to all lidar data collected between years 2000 and 2010. (b) For the data collected during the time period 2010–2016, we applied the automatic processing scheme of the Single Calculus Chain (SCC) (D'amico et al., 2016;

Mattis et al., 2016). The SCC code acts as an integrated and homogenized common processing chain which allows the automatic retrieval of the b_{aer} and a_{aer} coefficient profiles over the European continent, based on well-tested retrieval algorithms previously developed within EARLINET (Böckmann et al., 2004). Moreover, the SCC is highly configurable and can be easily adapted to analyze data coming from new lidar systems. The aerosol optical products of the SCC are evaluated (and error bars are calculated) with validated EARLINET measurements (D'amico et al., 2015; D'amico et al., 2016; Wandinger et al., 2016). For the case of the EOLE system, the evaluation of the manually retrieved aerosol optical properties has been performed against those retrieved by the SCC with very successful results during an intercomparison campaign organized, recently, in Athens (Amodeo et al., 2017), between the EOLE and the EARLINET reference system MUSA (Multi-wavelength System for Aerosol) (Madonna et al., 2011).

In this paper, the main emphasis has been given on the study of the mean aerosol optical properties retrieved only at 355 nm, since at this wavelength we have the longest database on the aerosol properties over Athens (from year 2000–2016) against the shorter available records at 532 nm (from year 2010–2016). We used 30′ to 60′ time averaging windows to retrieve the mean profiles of the aerosol properties, depending mainly on the prevailing atmospheric conditions, following the EARLINET standards (D'amico et al., 2015; D'amico et al., 2016). Furthermore, three criteria were applied to our dataset in order to select the "Saharan dust" profiles for our analysis: i) the aerosol profile should contain at least one distinct aerosol layer above the PBL height (Matthais et al., 2004b), ii) 5-day air mass back-trajectory analysis should overpass the Saharan dust region below certain height, and iii) supplementary datasets (e.g. from sunphotometers and satellite data) are also taken into account as an auxiliary indicators of dust predominance in the atmospheric column under study (Mona et al., 2006).

2.3. FLEXPART and BSC-DREAM8b model

To obtain a general idea about the origin of the air masses arriving over the Greater Athens Area (GAA) during the measurement dates, we performed air-mass back-trajectory analysis using the Flexible Particle Dispersion Model (FLEXPART), based on Global Data Assimilation System (GDAS) data, in order to provide sensitivity (residence time) plumes (Stohl and Thomson, 1999; Stohl et al., 1998, 2005; Seibert and Frank, 2004). Specifically, 7-day backward runs for releases of 40,000 air parcels every 3 h at 2000–4000 m a.s.l. were obtained by the FLEXPART model. Residence time (sensitivity) in grid cells above 4000 m a.s.l. is excluded, as the grid cells that might have pollutants in that height cannot be considered as aerosol source areas. FLEXPART takes into account not only grid scale wind (as simple trajectory models do) but also turbulent wind fluctuations and mesoscale wind fluctuations. It also incorporates drift correction (to prevent accumulation of computational particles released) and density correction (to account for the decrease of air density with height). FLEXPART model can be used to calculate with accuracy backward sensitivity plumes for periods as long as 30 days, in order to assess the impact of remote source areas.

Moreover, we used the Dust Regional Atmospheric Model BSC/DREAM8b (Basart et al., 2012) in order to predict and identify the transport of dust plumes over Athens, based on forecasted dust optical depth (at 550 nm). The BSC/DREAM8b model, operated by the Barcelona Supercomputer Center–(BSC-CNS: www.bsc.es) simulates all major processes of the atmospheric cycle of the mineral dust aerosol by solving the Euler-type partial differential nonlinear equation for dust mass continuity. The resolution of the model is set to 50 km in the horizontal and to 15 km in the vertical. This model is one of the most widely used ones for dust studies over the European continent (Papayannis et al., 2008; Amiridis et al., 2013; Huneeus et al., 2015; Tsekeri et al., 2017).

3. Results

3.1. Dust climatology: observations versus predictions

The schedule of the EOLE measurements during Saharan dust outbreaks (Papayannis et al., 2005, 2008) are based on early warnings, using forecasted data, provided by the BSC-DREAM8b model (Basart et al., 2012). The identification of the dust cases is based mainly on AOD values from sun photometer data over Athens (https://aeronet.gsfc.nasa.gov) and satellite Moderate Resolution Imaging Spectroradiometer (MODIS) observations (https://worldview.earthdata.nasa.gov). In Fig. 1a we present the monthly evolution of the number of dust cases observed by EOLE (only under clear weather conditions) and predicted by DREAM, for the period 2000–2016. The maximum number of occurrence of the dust days occurs to be within May, in both predicted (~30 cases) and observed cases (~16 cases), while the majority of the dust cases is observed between early spring (March) to late autumn (October). Specifically, 95% of the observed cases and 81% of the predicted ones, fall within this period. A minimum of occurrence appears during the winter months, due to the prevailing northeastern flow over Athens during this period (Kassomenos et al., 1995; Papayannis et al., 2008; Banks et al., 2016). However, the fact that the number of observed dust days is always fewer than the forecasted ones, can be attributed to the inability of the lidar technique to perform measurements under cloudy atmospheric conditions. Moreover, we found a quite strong correlation (determination coefficient: $R^2 = 0.81$) between

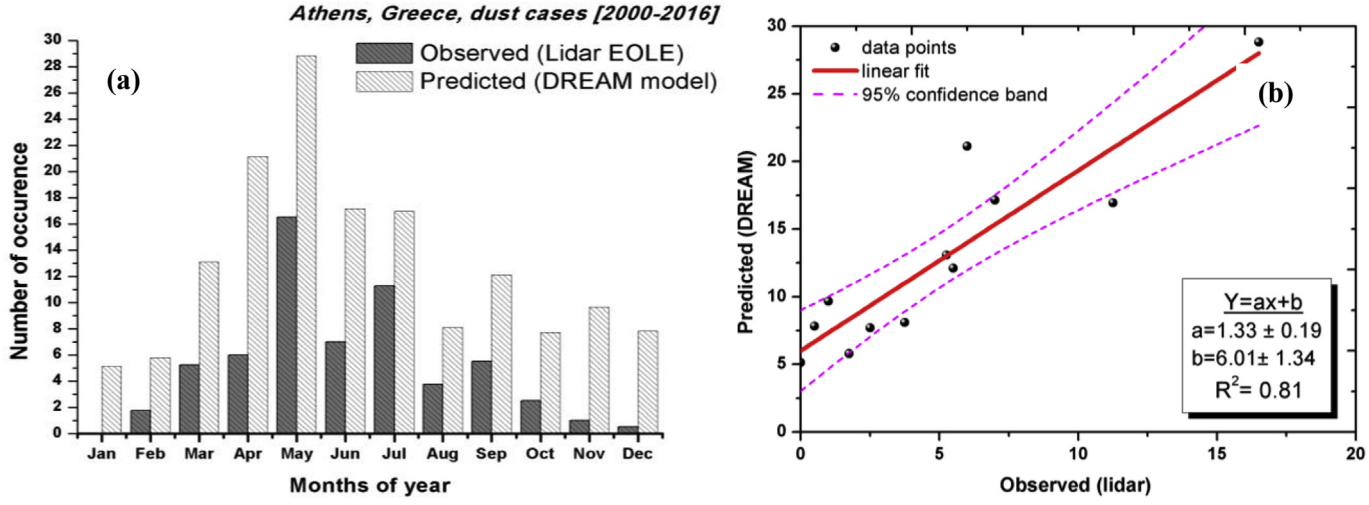

Fig. 1. Monthly evolution (a) and linear fit (b) of the mean number of dust cases observed (EOLE) and predicted (DREAM8b) for the period 2000–2016.

the occurrences of the observed and forecasted number of monthly mean cases, denoting their linear association (Fig. 1b). Roughly, about the half of the forecasted dust cases are finally observed by the lidar system during the studied time period (2000–2016). This means that in the worst case scenario, at least the 50% of the forecasted by the model dust events will be finally observed with EOLE, over the cloudless sky of Athens.

3.2. Dust optical properties

In Fig. 2a and b we present the seasonal variation (from spring to winter) of the vertical profiles (black lines) of the aerosol optical properties (backscatter (b_{aer}) and extinction (a_{aer}) coefficients) at 355 nm, as well as their mean values (red lines) and the corresponding statistical error expressed by the standard deviation (std) of the mean seasonal vertical profile (magenta vertical error bars). Similarly, the seasonal variation of the lidar ratios and their corresponding mean values are presented in Fig. 2c in the height range between 2000 and 4000 m, where usually most of the Saharan dust layers are observed (Papayannis et al., 2008). All these profiles show a quite large variability which is due to the varying intensity (due to different air mass trajectories) of the dust events occurring over Athens, as already discussed in Papayannis et al. (2008). The mean lidar ratio values within the dust plumes (spring: 58 ± 9 sr, summer: 57 ± 9 sr, autumn: 41 ± 9 sr, winter: 45 ± 6 sr) vary from season to season, with lower lidar ratio values during the colder months. This leads us to the conclusion that not only the time of long-range transport, but also the transport paths and the atmospheric conditions vary among seasons, which may affect the dust layer itself.

The frequency distribution of the lidar ratio values, calculated within the Saharan dust layers, at 355 nm (57 cases) is shown in Fig. 3. This distribution clearly shows a maximum occurrence at 40–50 sr (37% of cases) with the majority of cases lying between 42 and 62 sr (25%–75%), as shown in the inset boxplot of Fig. 3. More precisely, the mean value of the lidar ratio at 355 nm was found to be 52 ± 13 sr (with min. of 22 sr and max. of 77 sr) in the height range 2000–4000 m a.s.l. These large standard deviation values and the outliers of the boxplot indicate, for many cases, a possible mixture of dust with other

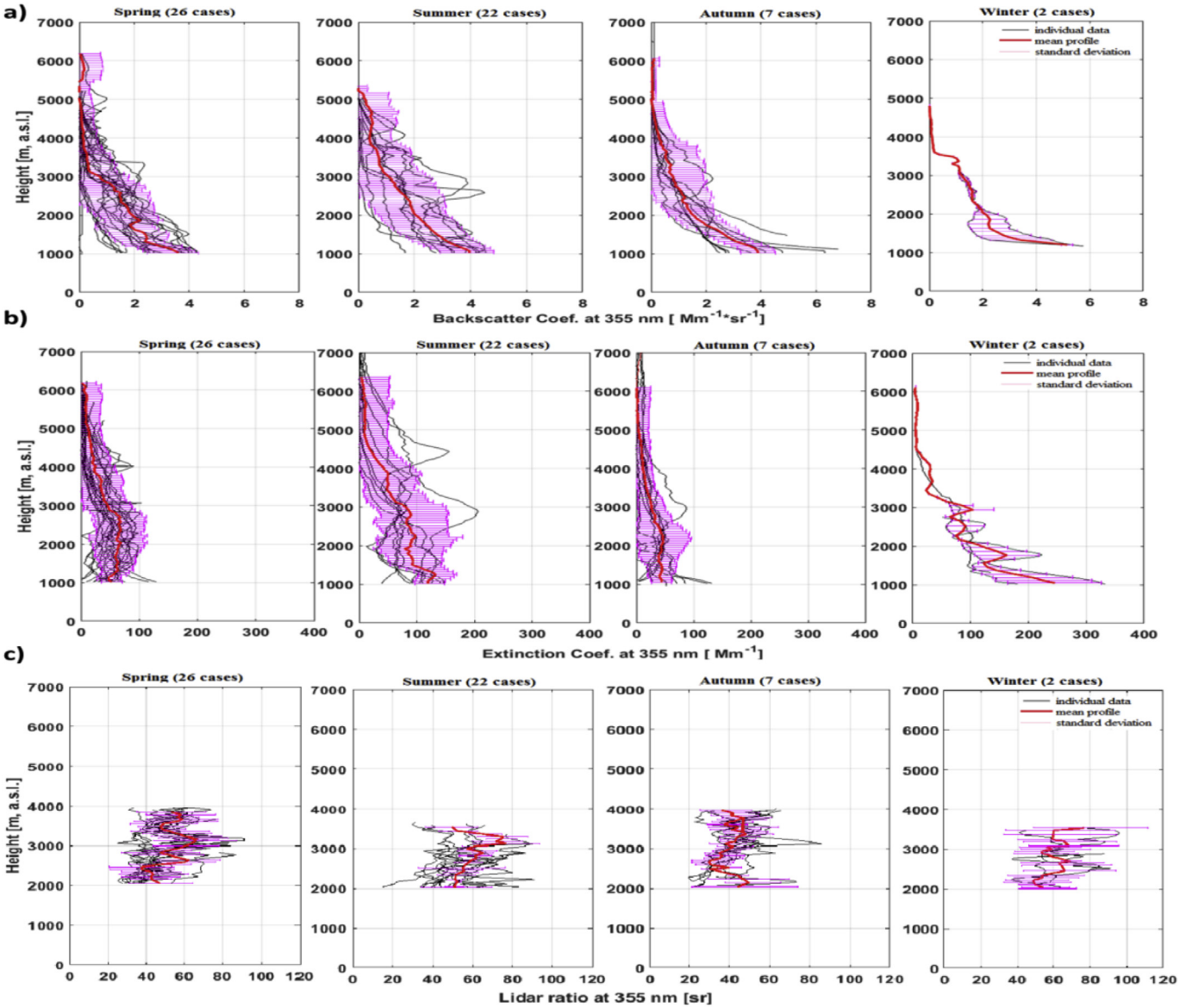

Fig. 2. Seasonal variation of the vertical profiles of the aerosol optical properties: a) b_{aer}, b) a_{aer} and c) lidar ratio, at 355 nm, as well as their mean values (red lines) and the corresponding statistical error (red error bars) for 57 dust cases during the period 2000–2016. (For interpretation of the references to colour in this figure legend, the reader is referred to the Web version of this article.)

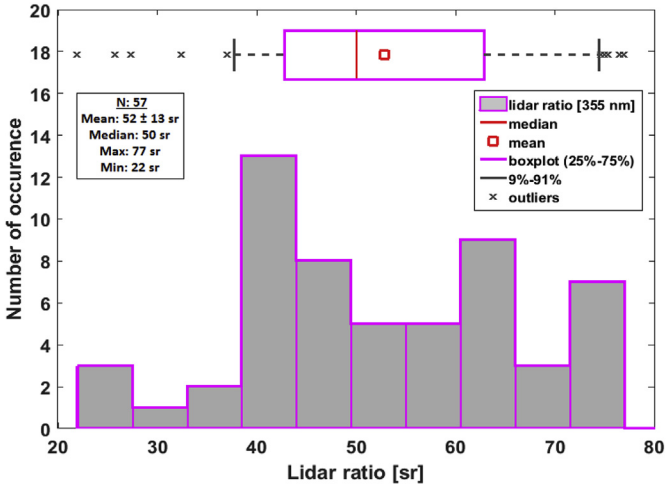

Fig. 3. Histogram and boxplot of the occurrence of lidar ratio values (sr) for 57 dust cases during the period 2000–2016, at 355 nm, calculated for heights between 2000 and 4000 m.

aerosol types (e.g. marine, polluted continental, and/or biomass burning ones), similarly shown by Groß et al. (2013).

The seasonal variability of the AOD values at 355 nm is demonstrated in Fig. 4. For each season the AOD values were obtained by vertically integrating the corresponding a_{aer} profiles inside the Saharan dust layer. In the box plot of this Figure, the box spans the interquartile range (IQR) from 25% to 75% percentile including the median line and the whiskers are chosen maximally 1.5× IQR away from the box. In this way, we can discern outsiders, shown as asterisks. It is clear that the AOD shows a significant seasonal variability, with minimum mean values (squared symbols) during autumn and maximum mean values in spring and summer months. These minimum and maximum levels of AODs are consistent with the seasonal Saharan dust outbreaks, in accordance with the seasonal variation observed over Athens by Papayannis et al. (2009), but at 532 nm. Moreover, the medians (vertical lines) of spring and summer are lower than the corresponding mean values, a fact that indicates that the distribution is skewed to lower values, but there are some exceptionally large ones. These values correspond to extreme dust episodes occurring during the above mentioned period. On the other hand, during the autumn and winter months, the distribution of the AOD values seems to be more normal, as the corresponding mean and median values are about the same. Regarding the AOD seasonal variability, the AOD values lay in a wide range during the hotter months (spring, summer), while during the colder months (autumn, winter) the variation remains smaller. The average AOD at 355 nm over the entire period (2000–2016) was 0.26 ± 0.16, ranging between a minimum of 0.003 and a maximum of 0.86.

The seasonal variability of the mean lidar ratio values, along with their standard deviation, at 355 nm, is shown in Fig. 5. The mean lidar ratio values within the dust plumes range from 41 sr (in autumn) to 58 sr (in spring). In fact, the springtime and summertime mean values along with their standard deviation values (58 ± 9 and 54 ± 9 sr, respectively) are very close to the ones (nearly pure dust) measured in situ during the SAMUM experiment (53 ± 5 sr, at 355 nm, as shown by Groß et al., 2015), which indicates a very low mixing of dust (strong dust events with a very fast (1–2 days) transport from the Saharan region to Athens passing over the Mediterranean and the Ionian Sea) with other types of particles during their transport from the Saharan desert to Athens. For the specific cases analyzed here, the autumn and winter mean values (41 ± 9 and 45 ± 6 sr, respectively) are lower than those observed during spring and summer and remain within those (40–45 sr) reported by Amiridis et al. (2005), Mueller et al. (2007) and Papayannis et al. (2008), possibly due to mixing with continental air masses and different transport paths. For instance, during the autumn period the air masses start from the central and western Saharan region, pass over Spain, Italy and the Balkans within a 2–3 days period, where they are enriched with continental particles, which typically show LR values around 40–45 sr (Mueller et al., 2007; Groß et al., 2013). Moreover, our data reveal a clear seasonal downtrend ($R^2 = 0.69$) in dust episode occurrences originating from Saharan desert from spring to winter, according to Fig. 5.

Additionally, no specific trends could be revealed during the reporting 16-year period, concerning the modification of dust pathways and dust quantities arriving over Athens based on the available air mass trajectory simulation data, except the aforementioned seasonal preference of the strongest dust transport during the springtime and summertime seasons. Therefore, it is obvious that not only the time spent over the long-range transport, but also the transport path and the atmospheric conditions that vary among seasons, may affect a dust layer itself.

3.3. Dust geometrical properties

In order to characterize the probed dust layers, in terms of their geometrical properties, parameters such as the layer base (z_B), layer top (z_T), layer thickness (th) and center of mass (z_{COM}), can be calculated from the lidar signals, following the procedure proposed by Mona et al. (2006). These parameters were calculated for each of our 57 selected dust cases. In Table 1 we present the height distribution of the mean, minimum and maximum values of the Saharan dust altitude-related parameters (z_B, z_T, th and z_{COM}) retrieved directly from the lidar b_{aer} data obtained at 355 nm over Athens, during the reported period (February 2000–December 2016). We found that multiple aerosol dust layers of variable thickness (609–6199 m) were observed. The z_{COM} of these layers was located in altitudes between 1270 and 5738 m with a mean value of 2699 ± 1017 m. The variability of the z_{COM} values could be related to the mixing of the different air masses arriving over our measuring site (Matthais et al., 2004a,b). The z_B of the dust layer ranged from around 926 m to a maximum of 5094 m, with a mean value of 1872 ± 845 m. Additionally, the z_T of the dust layer ranged from 2005 to 8014 m, with a mean value of the order of 4000 m.

The seasonal evolution of the z_B and z_T values indicates a mean minimum value during the autumn and winter months, which is related to the lower temperatures of the free troposphere, leading to cooler ground surfaces. On the contrary, during the hot period (spring and especially during summer months) these geometrical parameters show

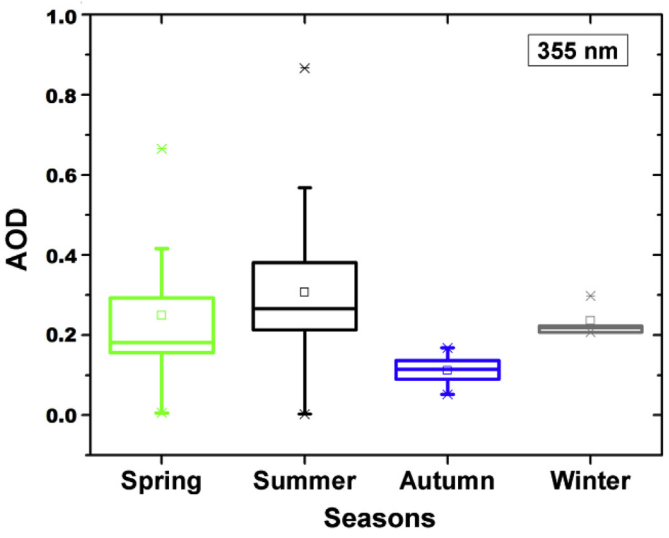

Fig. 4. Box plot of the seasonal variability of the mean AOD values as calculated at 355 nm for the period 2000–2016.

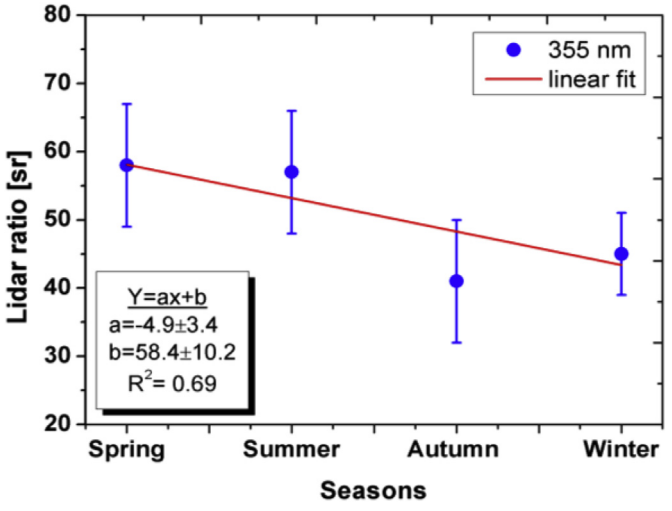

Fig. 5. Mean seasonal lidar ratio values at 355 nm during the period 2000–2016, between 2000 and 4000 m asl. height along with the linear fit of the mean values (red line). (For interpretation of the references to colour in this figure legend, the reader is referred to the Web version of this article.)

Table 1
Main characteristics of the Saharan dust retrieved from the baer profiles at 355 nm.

Years: 2000–2016	Mean	Maximum	Minimum
Base z_B (m)	1872 ± 845	5094	926
Top z_T (m)	4000 ± 1078	8014	2005
Thickness *th* (m)	2497 ± 1026	6199	987
Center of mass z_{com} (m)	2699 ± 1017	5738	1270

higher values (Fig. 6). Specifically, there is a downward trend of the mean seasonal z_B and z_T values from spring (z_B: 2150 m, z_T: 4560 m) to winter (z_B:1800 m, z_T: 3980 m). In summary, these observed trends could be related to: i) the different atmospheric conditions that prevail and characterize each season, ii) the occurrence of Saharan episodes over our area which is higher during spring and summer months, and iii) the convective activity which is strongest during the hot periods (mainly late spring and summer). Moreover, the mean seasonal *th* values present a relatively low standard deviation (rsd) equal to 9%, among the seasons.

3.4. Clustering analysis: origins of Saharan dust intrusions over Athens

A cluster analysis has been applied to all air mass trajectories arriving over our site in order to identify their origin using an algorithm based on Dorling (1992). The basic idea is that the non-hierarchical clustering algorithm generates a large number of "seed" trajectories, which cover the spread of the real trajectories used in the analysis and then, assigns each of the real trajectories to that seed which is closest in terms of the Euclidean distances between their corresponding 6-hourly coordinates. The user can define a percentage change in Root Mean Square Deviation (rmsd) which, when exceeded at some stage in the reduction of the number of clusters, signifies an optimum number of clusters to be retained in the analysis. The algorithm indicated these two optimum main clusters, with the corresponding average trajectories, called centroids (Toledano et al., 2009). Using these two "time clusters" the FLEXPART transport model was used in order to provide dust plumes on the basis of their residence time (expressed in hours) called sensitivity plumes (Stohl et al., 1998, 2005). Therefore, 7-day air mass back-trajectories were calculated from 0 to 500 m a.s.l. height over the source region, reaching over Athens between 2000 and 4000 m a.s.l., with a 3-h interval.

In Fig. 7, our clustering analysis reveals these two main clusters: one pathway from south-west to north-east, with dust emission areas in Algeria, Tunisia, and Libya (cluster A, linked with a low-pressure over Morocco and Algeria and a high-pressure over Libya-Egypt) and a second one from south, across the Mediterranean Sea with emission areas over Libya and the remaining part of Algeria and Tunisia (cluster B, linked with a low-pressure over Spain and a high-pressure over Libya-Egypt) in accordance with Moulin et al. (1998). Actually, the second cluster has similar pattern with the first one, except that it is more shifted to the east and north and has contribution from Europe. Moreover, Cluster B has a bigger number of air mass trajectories (60% of the cases) with lower lidar ratio values in comparison to Cluster A (40% of the cases) and its centroid is shifted more to the Mediterranean Sea.

Regarding the aerosol optical properties we found higher AOD values within cluster A (mean value of 0.39 ± 0.15) than within cluster B, at 355 nm. For cluster A the mean lidar ratio value was found to be 52 ± 15 sr, while for cluster B the mean AOD and lidar ratio values were found to be 0.32 ± 0.22 and 44 ± 15 sr, respectively. The difference in the values of these optical properties between the two clusters indicates that, although the origin does not differ much, the distance travelled and the residence time of the air masses, might differ. In order to verify this assumption, we calculated the air mass velocity within each cluster, correlating the distance travelled within 3-h interval along the clusters' centroid. Therefore, it is evident that the distance travelled and the residence time are both directly related to the air mass aging processes.

Indeed, as shown in Fig. 8, the air masses of cluster A remain 12 h more (dust enriched) over the African continent (75 h) than those of cluster B (63 h) and reach Athens faster (less mixing during transport) after a total travel time of 126 h. Concerning the time period spent over the Mediterranean Sea, the air masses of cluster A stay 51 h over that area, much less than the air masses of cluster B, which stay for about 78 h. As a consequence, the air masses of cluster B circulate ~27 h more over the Mediterranean Sea compared to those of Cluster A, thus, they mix more with marine aerosols within the first 500 m asl.

4. Conclusions

In this paper we presented a statistical analysis of the seasonal variability of the vertical profiles of the optical and geometrical properties of Saharan dust aerosols arriving over Athens (period 2000–2016) based on systematic aerosol multi-wavelength Raman lidar measurements under cloud-free conditions. This analysis was based on nighttime Raman measurements of range-resolved aerosol optical properties (backscatter and extinction coefficients, lidar ratio, and Ångström exponent) at 355 nm. We found a mean value of the lidar ratio inside the dust layers of the order of 52 ± 13 sr (355 nm) in the height region of 2000–4000 m. Moreover, multiple aerosol dust layers of variable thickness (609–6199 m) were observed at the same heights, with a mean thickness of 2497 ± 1026 m and a center of mass of 2699 ± 1017 m.

The occurrence of the predicted and observed dust events was highest during spring and summer months, less frequent during autumn and much less, during winter. The number of the forecasted dusty days (on monthly basis) by the BSC-DREAM8b model compared to those of the performed lidar measurements were found to have a quite strong correlation (R^2 = 0.81), with a maximum occurrence predicted for the spring season. In the worst case scenario, at least 50% of the model-forecasted dust events can be observed by lidar under cloudless skies over Athens. For the sampled dust plumes we found mean lidar ratios of 52 ± 13 sr at 355 nm in the height range 2000–4000 m a.s.l. Moreover, the dust layers had a mean thickness of 2497 ± 1026 m and a center of mass of 2699 ± 1017 m.

For the studied period, our air mass back-trajectory analysis delineated two main clusters: the first cluster (Cluster A) included air

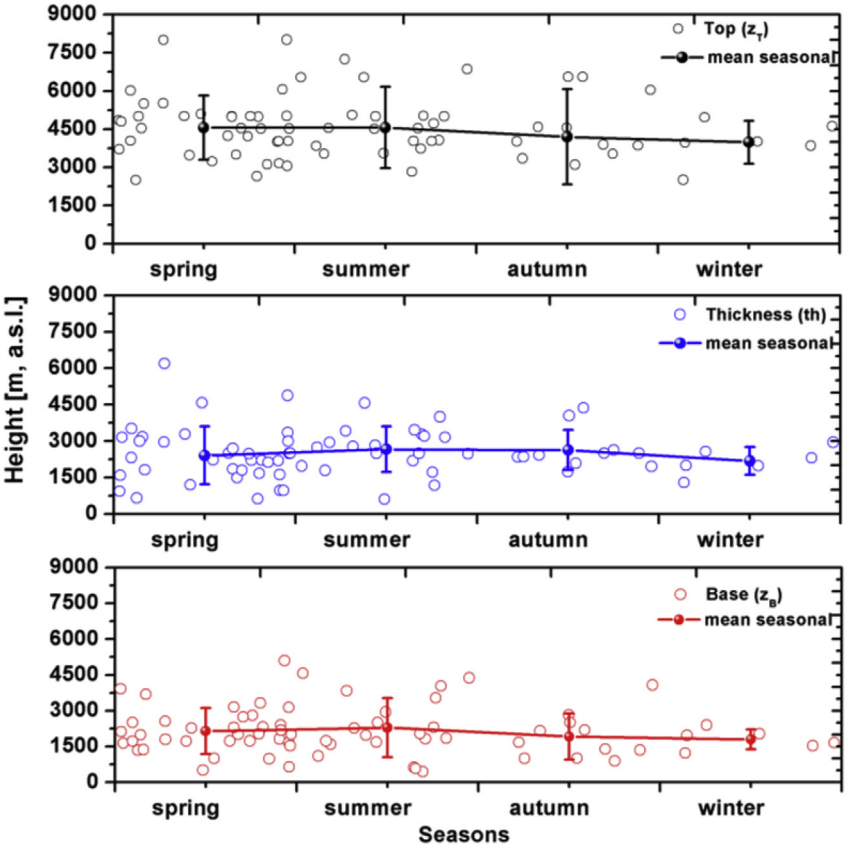

Fig. 6. Annual evolution of the layer properties: base z_B (lower part), thickness *th* (middle part) and top z_T (upper part) and their corresponding seasonal means with standard deviations for the 17 year period studied.

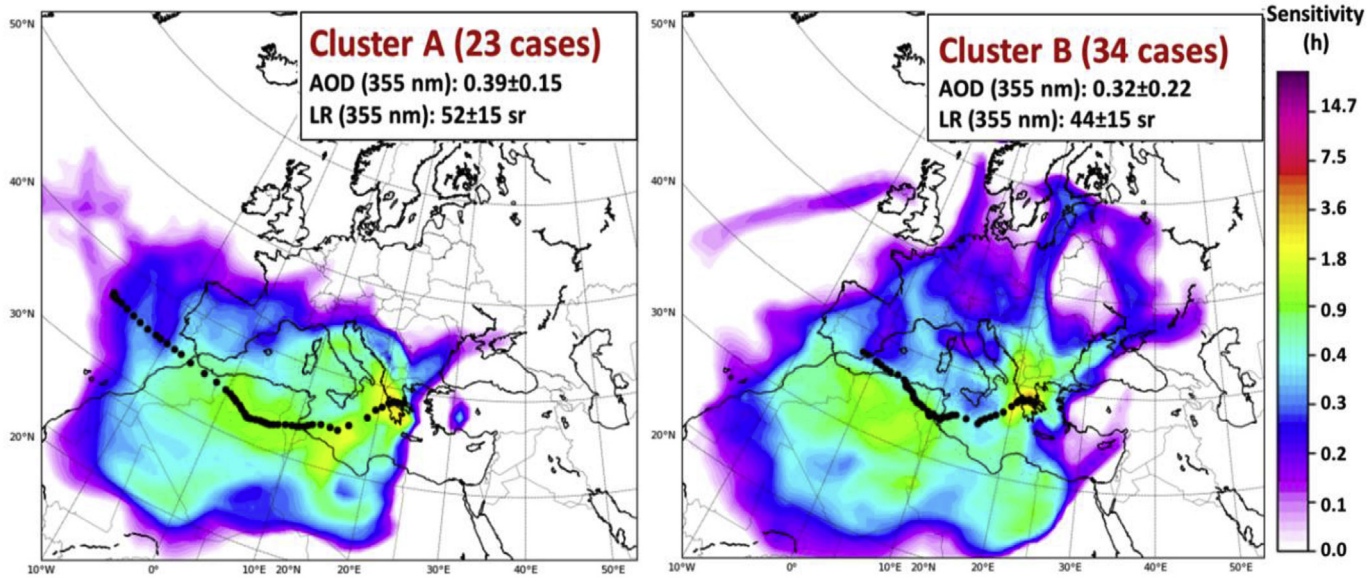

Fig. 7. 7-day air mass backward FLEXPART clusters for the 57 Saharan dust cases (2000–2016). Particles are released at a uniform rate during a 3-h interval from 0 to 500 m a.s.l. height reaching over Athens between 2000 and 4000 m. Left: Cluster A, Right: Cluster B. For each cluster, the centroids are presented (black dots) and the mean optical properties are mentioned (inset legend). The air mass residence time along the centroids' trajectory over each site is shown in hours. The charts are plotted with X axis (longitude) and Y axis (latitude).

masses coming from south-west to north-east (Tunisia, Algeria and Libya); the second cluster (Cluster B) included air masses coming from south/south-west, travelling across the Mediterranean Sea (Libya and the remaining part of Algeria and Tunisia). These air masses travelled at very low heights (0–500 m a.s.l.) along Africa and the Mediterranean Sea before reaching over Athens at heights between 2000 and 4000 m a.s.l.

This clustering enabled us to differentiate between the aerosol optical properties between the two clusters, based on their residence time over the Saharan region, the European continent and the Mediterranean

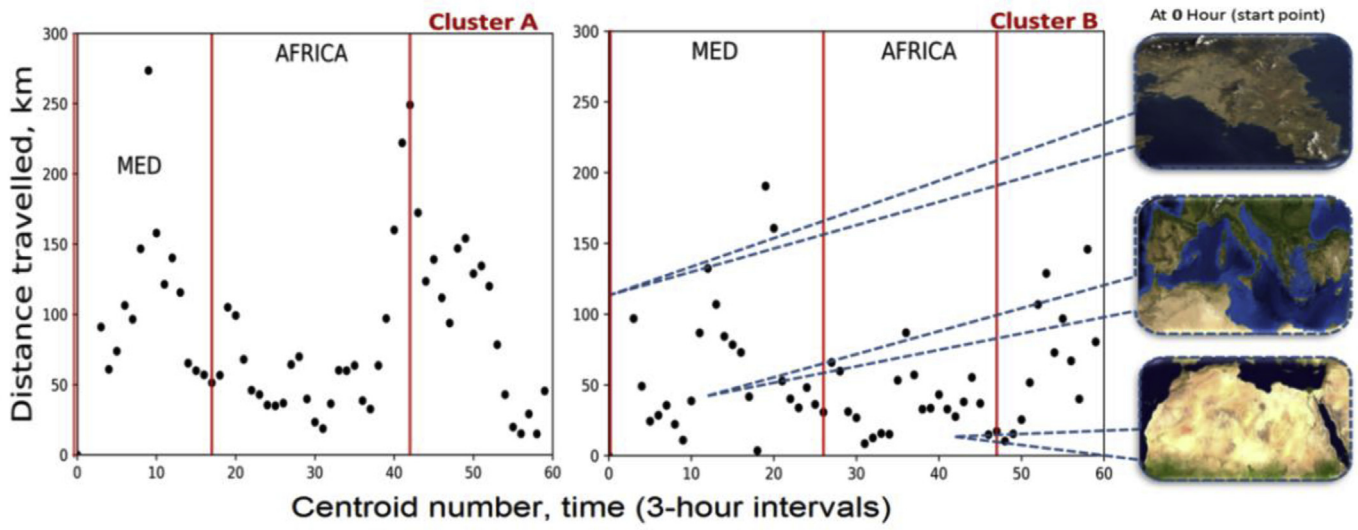

Fig. 8. Distance travelled (in km) every 3-h interval for the 7-day backward trajectory of each clusters' centroid: cluster A (left) and cluster B (right). Their residence time over Mediterranean and the African continent (red rectangulars) are mentioned by the black dots (each dot represents a 3-h interval). (For interpretation of the references to colour in this figure legend, the reader is referred to the Web version of this article.)

Sea. Specifically, we found higher mean values of AOD (0.39 ± 0.15 at 355 nm) for air the masses within cluster A in comparison to those within Cluster B (0.32 ± 0.22); regarding the LR values at 355 nm, these were lower within Cluster A (LR = 52 ± 15 sr) than within Cluster B (LR = 44 ± 15 sr). We have strengthened this indication by calculating the air mass velocity within each clusters' centroid and we found that the air masses of cluster B not only circulate over the Mediterranean Sea for about 27 h more than those of cluster A, but also, air masses of Cluster A remain 12 h more (dust enriched) over the African continent, than those of Cluster B. We concluded that even if the dust source regions are about the same, the aging and mixing processes of these air masses, passing over different areas, might have an impact on the aerosol optical properties, since the air masses of cluster B circulate ~27 h more over the Mediterranean Sea compared to those of Cluster A. Consequently, they mix more with marine aerosols within the first 500 m asl.

This paper contributes to the enrichment of the aerosol optical and geometrical properties database in the South-Eastern Europe for periods longer than fifteen years, which are very useful input data for the improvement of radiative transfer climatic models (Carslaw et al., 2013).

Acknowledgments

The research leading to these results has received funding from the European Union 6th and 7th Framework Programmes (FP6: grant agreement RICA-025991 and FP7: grant agreement 262254), as well as from the Horizon 2020 ACTRIS research/innovation programme under grant agreement n° 654109. AP and AA have received funding from the European Union 7th Framework Programme (FP7/2007–2013): People, ITN Marie Curie Actions Programme (2012–2016) in the frame of ITaRS, under grant agreement n° 289923. The dust forecasts have been provided by BSC-DREAM8b model (www.bsc.es/ESS/). We are also grateful to A. Stohl (NILU), G. Wotawa and P. Seibert (Institute of Meteorology and Geophysics, Vienna, Austria) and ECMWF (European Center for Medium Range Weather Forecast) for the provision of FLEXPART model and MARS reanalysis meteorological data, respectively. This research project has been financed through a scholarship (grant number 979) from the General Secretariat for Research and Technology and Hellenic Foundation for Research and Innovation (HFRI).

Appendix A. Supplementary data

Supplementary data related to this article can be found at http://dx.doi.org/10.1016/j.atmosenv.2018.04.011.

References

Amiridis, V., Balis, D.S., Kazadzis, S., Bais, A., Giannakaki, E., Papayannis, A., Zerefos, C., 2005. Four-year aerosol observations with a Raman lidar at Thessaloniki, Greece, in the framework of European aerosol research lidar network (EARLINET). J. Geophys. Res. Atmos. 110. http://dx.doi.org/10.1029/2005JD006190.

Amiridis, V., Wandinger, U., Marinou, E., Giannakaki, E., Tsekeri, A., Basart, S., Kazadzis, S., Gkikas, A., Taylor, M., Baldasano, J., Ansmann, A., 2013. Optimizing CALIPSO Saharan dust retrievals. Atmos. Chem. Phys. 13, 12089–12106. http://dx.doi.org/10.5194/acp-13-12089-2013.

Amodeo, A., D'Amico, G., Giunta, A., Papagiannopoulos, N., Papayannis, A., Argyrouli, A., Mylonaki, M., Tsaknakis, G., Kokkalis, P., Soupiona, O., Tzanis, C., 2017. AthLi16: the Athens lidar intercomparison campaign. In: Proc. 28th International Laser Radar Conference, 25–30 June 2017, Bucharest, Romania.

Ansmann, A., Riebesell, M., Wandinger, U., Weitkamp, C., Voss, E., Lahmann, W., Michaelis, W., 1992. Combined Raman elastic-backscatter lidar for vertical profiling of moisture, aerosol extinction, backscatter, and lidar ratio. Appl. Phys. B 55, 18–28.

Atkinson, James D., Murray, Benjamin J., Woodhouse, Matthew T., Whale, Thomas F., Baustian, K.J., et al., 2013. The importance of feldspar for ice nucleation by mineral dust inmixed-phase clouds - ProQuest. Nature 498.

Balis, D., Amiridis, V., Kazadzis, S., Papayannis, A., Tsaknakis, G., Tzortzakis, S., Kalivitis, N., Vrekoussis, M., Kanakidou, M., Mihalopoulos, N., Chourdakis, G., Nickovic, S., Perez, C., Baldasano, J., Drakakis, M., 2006. Optical characteristics of desert dust over the East Mediterranean during summer. Ann. Geophys. 24.

Balis, D.S., Amiridis, V., Nickovic, S., Papayannis, A., Zerefos, C., 2004. Optical properties of Saharan dust layers as detected by a Raman lidar at Thessaloniki, Greece. Geophys. Res. Lett. 31, 10–13. http://dx.doi.org/10.1029/2004GL019881.

Banks, R.F., Tiana-Alsina, J., Baldasano, J.M., Rocadenbosch, F., Papayannis, A., Solomos, S., Tzanis, C.G., 2016. Sensitivity of boundary-layer variables to PBL schemes in the WRF model based on surface meteorological observations, lidar, and radiosondes during the HygrA-CD campaign. Atmos. Res. 176–177, 185–201. http://dx.doi.org/10.1016/j.atmosres.2016.02.024.

Basart, S., Pérez, C., Nickovic, S., Cuevas, E., Baldasano, J., 2012. Development and evaluation of the BSC-DREAM8b dust regional model over Northern Africa, the Mediterranean and the Middle East. Tellus B Chem. Phys. Meteorol. 64, 18539. http://dx.doi.org/10.3402/tellusb.v64i0.18539.

Böckmann, C., Wandinger, U., Ansmann, A., Bösenberg, J., Amiridis, V., Boselli, A., Delaval, A., De Tomasi, F., Frioud, M., Grigorov, I.V., Hågård, A., Horvat, M., Iarlori, M., Komguem, L., Kreipl, S., Larchevêque, G., Matthias, V., Papayannis, A., Pappalardo, G., Rocadenbosch, F., Rodrigues, J.A., Schneider, J., Shcherbakov, V., Wiegner, M., 2004. Aerosol lidar intercomparison in the framework of the EARLINET project 2 Aerosol backscatter algorithms. Appl. Optic. 43, 977. http://dx.doi.org/10.1364/AO.43.000977.

Bösenberg, J., Linne, H., Matthias, V., et al., 2003. A European Aerosol Research Lidar Network to Establish an Aerosol Climatology. Max-Planck Inst. fur Meteorol MPI Report.

Bösenberg, J., Timm, R., Wulfmeyer, V., 1997. Study of Retrieval Algorithms for a

Backscatter Lidar. Final Report, MPI Report No, vol. 226. pp. 1–66 Hamburg.
Carslaw, K.S., Lee, L.A., Reddington, C.L., Pringle, K.J., Rap, A., Forster, P.M., Mann, G.W., Spracklen, D.V., Woodhouse, M.T., Regayre, L.A., Pierce, J.R., 2013. Large contribution of natural aerosols to uncertainty in indirect forcing. Nature 503, 67–71. http://dx.doi.org/10.1038/nature12674.
D'amico, G., Amodeo, A., Baars, H., Binietoglou, I., Freudenthaler, V., Mattis, I., Wandinger, U., Pappalardo, G., 2015. EARLINET Single Calculus Chain – overview on methodology and strategy. Atmos. Meas. Tech. 8, 4891–4916. http://dx.doi.org/10.5194/amt-8-4891-2015.
D'amico, G., Amodeo, A., Mattis, I., Freudenthaler, V., Pappalardo, G., 2016. EARLINET Single Calculus Chain – technical – Part 1: pre-processing of raw lidar data. Atmos. Meas. Tech. 9, 491–507. http://dx.doi.org/10.5194/amt-9-491-2016.
Dorling, S.R., 1992. Cluster analysis: a technique for estimating the synoptic meteorological controls on air and precipitation chemistry–method and applications, Atmos. Environ. 26. pp. 2575–2581.
Dulac, F., Tanré, D., Bergametti, G., Buat-Ménard, P., Desbois, M., Sutton, D., 1992. Assessment of the African airborne dust mass over the western Mediterranean Sea using Meteosat data. J. Geophys. Res. Atmos. 97, 2489–2506. http://dx.doi.org/10.1029/91JD02427.
Dunion, J.P., Velden, C.S., Dunion, J.P., Velden, C.S., 2004. The impact of the Saharan air layer on Atlantic tropical cyclone activity. Bull. Am. Meteorol. Soc. 85, 353–365. http://dx.doi.org/10.1175/BAMS-85-3-353.
Evan, A.T., Flamant, C., Gaetani, M., Guichard, F., 2016. The past, present and future of African dust. Nature 531, 493–495.
Forster, P., Ramaswamy, V., Artaxo, P., Berntsen, T., Betts, R., Fahey, D.W., Haywood, J., Lean, J., Lowe, D.C., Myhre, G., Nganga, J., Prinn, R., Raga, G., Schulz, M., Van, R., 2007. Changes in Atmospheric Constituents and in Radiative Forcing Changes in Atmospheric Constituents and in Radiative Forcing Chapter 2. Netherlands. G. Bodeker (New Zealand) Clim. Chang.
Freudenthaler, V., 2008. The telecover test: a quality assurance tool for the optical part of a lidar system. In: Proc. 24th International Laser Radar Conference, 23–27 June 2008, Boulder, CO, USA, S01P-3.
Gkikas, A., Houssos, E.E., Lolis, C.J., Bartzokas, A., Mihalopoulos, N., Hatzianastassiou, N., 2015. Atmospheric circulation evolution related to desert-dust episodes over the Mediterranean. Q. J. R. Meteorol. Soc. 141, 1634–1645. http://dx.doi.org/10.1002/qj.2466.
Groß, S., Esselborn, M., Weinzierl, B., Wirth, M., Fix, A., Petzold, A., 2013. Aerosol classification by airborne high spectral resolution lidar observations. Atmos. Chem. Phys. 13, 2487–2505.
Groß, S., Freudenthaler, V., Schepanski, K., Toledano, C., Schäfler, A., Ansmann, A., Weinzierl, B., 2015. Optical properties of long-range transported Saharan dust over Barbados as measured by dual-wavelength depolarization Raman lidar measurements. Atmos. Chem. Phys. 15, 11067–11080. http://dx.doi.org/10.5194/acp-15-11067-2015.
Hamonou, E., Chazette, P., Balis, D., Dulac, F., Schneider, X., Galani, E., Ancellet, G., Papayannis, A., 1999. Characterization of the vertical structure of Saharan dust export to the Mediterranean basin. J. Geophys. Res. Atmos. 104, 22257–22270. http://dx.doi.org/10.1029/1999JD900257.
Holben, B.N., Tanré, D., Smirnov, A., Eck, T.F., Slutsker, I., Abuhassan, N., Newcomb, W.W., Schafer, J.S., Chatenet, B., Lavenu, F., Kaufman, Y.J., Castle, J. Vande, Setzer, A., Markham, B., Clark, D., Frouin, R., Halthore, R., Karneli, A., O'Neill, N.T., Pietras, C., Pinker, R.T., Voss, K., Zibordi, G., 2001. An emerging ground-based aerosol climatology: aerosol optical depth from AERONET. J. Geophys. Res. Atmos. 106, 12067–12097. http://dx.doi.org/10.1029/2001JD900014.
Huneeus, N., Basart, S., Fiedler, S., Morcrette, J.J., Benedetti, A., Mulcahy, J., Terradellas, E., Perez, C.G.P., Pejanovic, G., Nickovic, S., Arsenovic, P., Schulz, M., Cuevas, E., Baldasano, J.M., Pey, J., Remy, S., Cvetkovic, B., 2015. Forecasting the north African dust outbreak towards Europe in April 2011: a model intercomparison. Atmos. Chem. Phys. 15, 26661–26710.
Intergovernmental Panel on Climate Change, 2014. Clouds and aerosols. In: Climate Change 2013 – The Physical Science Basis: Working Group I Contribution to the Fifth Assessment Report of the Intergovernmental Panel on Climate Change. Cambridge University Press, Cambridge, pp. 571–658. http://dx.doi.org/10.1017/CBO9781107415324.016.
Karydis, V.A., Tsimpidi, A.P., Bacer, S., Pozzer, A., Nenes, A., Lelieveld, J., 2017. Global impact of mineral dust on cloud droplet number concentration. Atmos. Chem. Phys. 17, 5601–5621. http://dx.doi.org/10.5194/acp-17-5601-2017.
Kassomenos, P., Kotroni, V., Kallos, G., 1995. Analysis of climatological and air quality observations from Greater Athens area. Atmos. Environ. 29B, 3671–3688.
Klett, J.D., 1985. Lidar inversion with variable backscatter/extinction ratios. Appl. Optic. 24 (11), 1638–1643. http://dx.doi.org/10.1364/AO.24.001638.
Klett, J.D., 1981. Stable analytical inversion solution for processing lidar returns. Appl. Optic. 20, 211. http://dx.doi.org/10.1364/AO.20.000211.
Knippertz, P., Todd, M.C., 2012. Mineral dust aerosols over the Sahara: meteorological controls on emission and transport and implications for modeling. Rev. Geophys. 50. http://dx.doi.org/10.1029/2011RG000362.
Kokkalis, P., Papayannis, A., Mamouri, R.E., Tsaknakis, G., Amiridis, V., 2012. The EOLE lidar system of the national technical university of Athens. In: 26th International Laser Radar Conference, June 25-29, 2012, Porto Heli, Greece.
Kokkalis, P., 2017. Using paraxial approximation to describe the optical setup of a typical EARLINET lidar system. Atmos. Meas. Tech. 10, 3103–3115. http://dx.doi.org/10.5194/amt-10-3103-2017.
Landulfo, E., Moreira, D.S., Jorge, M.P.M.P., 2007. Tropospheric aerosol observations in São Paulo, Brazil using a compact lidar system. http://dx.doi.org/10.1080/01431160500033971.
Madonna, F., Amodeo, A., Boselli, A., Cornacchia, C., Cuomo, V., D'Amico, G., Giunta, A., Mona, L., Pappalardo, G., 2011. CIAO: the CNR-IMAA advanced observatory for atmospheric Research. Atmos. Meas. Tech. 4, 1191–1208.
Marinou, E., Amiridis, V., Binietoglou, I., Tsikerdekis, A., Solomos, S., Proestakis, E., Konsta, D., Papagiannopoulos, N., Tsekeri, A., Vlastou, G., Zanis, P., Balis, B., Wandinger, U., Ansmann, A., 2017. Three-dimensional evolution of Saharan dust transport towards Europe based on a 9-year EARLINET-optimized CALIPSO dataset. Atmos. Chem. Phys. 17, 5893–5919.
Matthais, V., Freudenthaler, V., Amodeo, A., Balin, I., Balis, D., Bösenberg, J., Chaikovsky, A., Chourdakis, G., Comeron, A., Delaval, A., De Tomasi, F., Eixmann, R., Hågård, A., Komguem, L., Kreipl, S., Matthey, R., Rizi, V., Rodrigues, J.A., Wandinger, U., Wang, X., 2004a. Aerosol lidar intercomparison in the framework of the EARLINET project. 1. Instruments. Appl. Opt. 43, 961–976.
Matthias, V., Balis, D., Bösenberg, J., Eixmann, R., Iarlori, M., Komguem, L., Mattis, I., Papayannis, A., Pappalardo, G., Perrone, M.R., Wang, X., 2004b. Vertical aerosol distribution over Europe: statistical analysis of Raman lidar data from 10 European aerosol research lidar network (EARLINET) stations. J. Geophys. Res. Atmos. 109. http://dx.doi.org/10.1029/2004JD004638.
Mattis, I., Ansmann, A., Müller, D., Wandinger, U., Althausen, D., 2002. Dual-wavelength Raman lidar observations of the extinction-to-backscatter ratio of Saharan dust. Geophys. Res. Lett. 29, 20–21. http://dx.doi.org/10.1029/2002GL014721.
Mattis, I., D 'amico, G., Baars, H., Amodeo, A., Madonna, F., Iarlori, M., 2016. EARLINET Single Calculus chain – technical – Part 2: calculation of optical products. Atmos. Meas. Tech. 9, 3009–3029. http://dx.doi.org/10.5194/amt-9-3009-2016.
Mattis, I., Müller, D., Ansmann, A., Wandinger, U., Preißler, J., Seifert, P., Tesche, M., 2008. Ten years of multiwavelength Raman lidar observations of free-tropospheric aerosol layers over central Europe: geometrical properties and annual cycle. J. Geophys. Res. Atmos. 113. http://dx.doi.org/10.1029/2007JD009636.
Mona, L., Amodeo, A., Pandolfi, M., Pappalardo, G., 2006. Saharan dust intrusions in the Mediterranean area: three years of Raman lidar measurements. J. Geophys. Res. Atmos. 111, 1–13. http://dx.doi.org/10.1029/2005JD006569.
Moulin, C., Dulac, F., Lambert, C.E., Chazette, P., Jankowiak, I., Chatenet, B., Lavenu, F., 1997a. Long-term daily monitoring of Saharan dust load over ocean using Meteosat ISCCP-B2 data: 2. Accuracy of the method and validation using Sun photometer measurements. J. Geophys. Res. Atmos. 102, 16959–16969. http://dx.doi.org/10.1029/96JD02598.
Moulin, C., Lambert, C.E., Dulac, F., Dayan, U., 1997b. Control of atmospheric export of dust from north Africa by the north Atlantic oscillation. Nature 387, 691–694. http://dx.doi.org/10.1038/42679.
Moulin, C., Lambert, C.E., Dayan, U., Masson, V., Ramonet, M., Bousquet, P., Legrand, M., Balkanski, Y.J., Guelle, W., Marticorena, B., Bergametti, G., Dulac, F., 1998. Satellite climatology of African *dust* transport in the Mediterranean atmosphere. J. Geophys. Res. 103. http://dx.doi.org/10.1029/98JD00171.
Mueller, D., Ansmann, A., Mattis, I., Tesche, M., Wandinger, U., Althausen, D., Pisani, G., 2007. Aerosol-type-dependent lidar ratios observed with Raman lidar. J. Geophys. Res. 112, D16202. http://dx.doi.org/10.1029/2006JD008292.
Müller, D., Böckmann, C., Kolgotin, A., Schneidenbach, L., Chemyakin, E., Rosemann, J., Znak, P., Romanov, A., 2016. Microphysical particle properties derived from inversion algorithms developed in the framework of EARLINET. Atmos. Meas. Tech. 9, 5007–5035. http://dx.doi.org/10.5194/amt-9-5007-2016.
Murayama, T., Sugimoto, N., Uno, I., Kinoshita, K., Aoki, K., Hagiwara, N., Liu, Z., Matsui, I., Sakai, T., Shibata, T., Arao, K., Sohn, B., Won, J., Yoon, S., Li, T., Zhou, J., Hu, H., Abo, M., Iokibe, K., Koga, R., Iwasaka, Y., 2001. Ground-based network observation of Asian dust events of April 1998 in east Asia. J. Geophys. Res. Atmos. 106, 18345–18359. http://dx.doi.org/10.1029/2000JD900554.
Papayannis, A., Amiridis, V., Mona, L., Tsaknakis, G., Balis, D., Bösenberg, J., Chaikovski, A., Tomasi, F., De, Grigorov, I., Mattis, I., Mitev, V., Müller, D., Nickovic, S., Pérez, C., Pietruczuk, A., Pisani, G., Ravetta, F., Rizi, V., Sicard, M., Trickl, T., Wiegner, M., Gerding, M., Mamouri, R.E., D'Amico, G., Pappalardo, G., 2008. Systematic lidar observations of Saharan dust over Europe in the frame of EARLINET (2000–2002). J. Geophys. Res. Atmos. 113. http://dx.doi.org/10.1029/2007JD009028.
Papayannis, A., Balis, D., Amiridis, V., Chourdakis, G., Tsaknakis, G., Zerefos, C., Castanho, A.D.A., Nickovic, S., Kazadzis, S., Grabowski, J., 2005. Measurements of Saharan dust aerosols over the Eastern Mediterranean using elastic backscatter-Raman lidar, spectrophotometric and satellite observations in the frame of the EARLINET project. Atmos. Chem. Phys. 5, 2065–2079.
Papayannis, A., Mamouri, R.E., Amiridis, V., Kazadzis, S., Perez, C., Tsaknakis, G., Kokkalis, P., Baldasano, J.M., 2009. Systematic lidar observations of Saharan dust layers over Athens, Greece in the frame of EARLINET project (2004–2006). Physics Ann. Geophys. 27, 3611–3620.
Papayannis, A., Mamouri, R.E., Chourdakis, G., Georgoussis, G., Amiridis, A., Paronis, D., Tsaknakis, G., Avdikos, G., 2007. Retrieval of the optical properties of tropospheric aerosols over Athens, Greece combining a 6-wavelength Raman-lidar and the CALIPSO VIS-NIR lidar system: case-study analysis of a Saharan dust intrusion over the Eastern Mediterranean. J. Optoelectron. Adv. Mater. 9, 3514–3517.
Papayannis, A., Nicolae, D., Kokkalis, P., Binietoglou, I., Talianu, C., Belegante, L., Tsaknakis, G., Cazacu, M.M., Vetres, I., Ilic, L., 2014. Optical, size and mass properties of mixed type aerosols in Greece and Romania as observed by synergy of lidar and sunphotometers in combination with model simulations: a case study. Sci. Total Environ. 500–501, 277–294. http://dx.doi.org/10.1016/j.scitotenv.2014.08.101.
Pappalardo, G., Amodeo, A., Apituley, A., Comeron, A., Freudenthaler, V., Linné, H., Ansmann, A., Bösenberg, J., D 'amico, G., Mattis, I., Mona, L., Wandinger, U., Amiridis, V., Alados-Arboledas, L., Nicolae, D., Wiegner, M., 2014. EARLINET: towards an advanced sustainable European aerosol lidar network. Atmos. Meas. Tech. 7, 2389–2409. http://dx.doi.org/10.5194/amt-7-2389-2014.
Prospero, J.M., 1996. Saharan Dust Transport over the North Atlantic Ocean and the Mediterranean, in the Impact of Desert Dust across the Mediterranean. Springer, New

York.
Prospero, J.M., Ginoux, P., Torres, O., Nicholson, S.E., Gill, T.E., 2002. Environmental characterization of global sources of atmospheric soil dust identified with the nimbus 7 total ozone mapping spectrometer (TOMS) absorbing aerosol product. Rev. Geophys. 40, 1–2. http://dx.doi.org/10.1029/2000RG000095.
Samaras, S., Nicolae, D., Böckmann, C., Vasilescu, J., Binietoglou, I., Labzovskii, L., Toanca, F., Papayannis, A., 2015. Using Raman-lidar-based regularized microphysical retrievals and Aerosol Mass Spectrometer measurements for the characterization of biomass burning aerosols. J. Comput. Phys. 299, 156–174. http://dx.doi.org/10.1016/j.jcp.2015.06.045.
Seibert, P., Frank, A., 2004. Source-receptor matrix calculation with a Lagrangian particle dispersion model in backward mode. Atmos. Chem. Phys. 4, 51–63.
Seinfeld, J., Bretherton, C., Carslaw, K.S., Coe, H., DeMott, P.J., Dunlea, E.J., Feingold, G., Ghan, S., Guenther, A.B., Kahn, R., Kraucunas, I., Kreidenweis, S.M., Molina, M.J., Nenes, A., Penner, J.F., Prather, K.A., Ramanathan, V., Ramaswamyy, V., Rasch, P.J., Ravishankara, A.R., Rosenfeld, D., Stephens, G., Wood, R., 2016. Improving our fundamental understanding of the role of aerosol−cloud interactions in the climate system. Proc. Natl. Acad. Sci. U.S.A. 113, 5781–5790. http://dx.doi.org/10.1073/pnas.1514043113.
Stohl, A., Forster, C., Frank, A., Seibert, P., Wotawa, G., 2005. Technical note: the Lagrangian particle dispersion model FLEXPART version 6.2. Atmos. Chem. Phys. 5, 2461–2474.
Stohl, A., Hittenberger, M., Wotawa, G., 1998. Validation of the Lagrangian particle dispersion model FLEXPART against large-scale tracer experiment data. Atmos. Environ. 32, 4245–4264.
Stohl, A., Thomson, D.J., 1999. A density correction for Lagrangian particle dispersion models. Boundary-Layer Meteorol. 90, 155–167.
Toledano, C., Cachorro, V.E., De Frutos, A.M., Torres, B., Berjon, A., Sorribas, M., Stone, R.S., 2009. Airmass classification and analysis of aerosol types at El Arenosillo (Spain). J. Appl. Meteor. Climat. 48, 962–981.
Tsekeri, A., Amiridis, V., Kokkalis, P., Basart, S., Chaikovsky, A., Dubovik, O., Mamouri, R.E., Papayannis, A., Baldasano, J.M., 2013. Application of a Synergetic Lidar and Sunphotometer Algorithm for the Characterization of a Dust Event over Athens, Greece, vol. 3. pp. 531–546. http://dx.doi.org/10.9734/BJECC/2013/2615.
Tsekeri, A., Lopatin, A., Amiridis, V., Marinou, E., Igloffstein, J., Siomos, N., Solomos, S., Kokkalis, P., Engelmann, R., Baars, H., Gratsea, M., Raptis, P.I., Binietoglou, I., Mihalopoulos, N., Kalivitis, N., Kouvarakis, G., Bartsotas, N., Kallos, G., Basart, S., Schuettemeyer, D., Wandinger, U., Ansmann, A., Chaikovsky, A.P., Dubovic, O., 2017. GARRLiC and LIRIC: strengths and limitations for the characterization of dust and marine particles along with their mixtures. Atmos. Meas. Tech. 10, 4995–5016.
Wandinger, U., et al., 2016. EARLINET instrument intercomparison campaigns: overview on strategy and results. Atmos. Meas. Tech. 9, 1001–1023. http://dx.doi.org/10.5194/amt-9-1001-2016.
Zuev, V.V., Burlakov, V.D., Nevzorov, A.V., Pravdin, V.L., Savelieva, E.S., Gerasimov, V.V., 2017. 30-year lidar observations of the stratospheric aerosol layer state over Tomsk (Western Siberia, Russia). Atmos. Chem. Phys. 17, 3067–3081. http://dx.doi.org/10.5194/acp-17-3067-2017.